Electrodeposition of Nanostructured Nickel-Ceramic Composite Coatings: A review

Yahia H. Ahmad and Adel M. A. Mohamed[*]

Center for Advanced Materials, Qatar University, Doha 2713, Qatar, Fax: +974-4403-3889
[*]E-mail: adel.mohamed@qu.edu.qa

This review presents a recent literature on electrochemically prepared nickel-ceramic nanocomposites coatings. These nanostructured coatings exhibit remarkable enhanced corrosion resistance and microhardness which are of interest for applications in diverse fields. In this review article significant attention is paid to the mechanisms of metal-particle electrocodeposition and different parameters affecting the electrodeposition process. Different techniques used in characterization of these composite coatings were also considered.

1. INTRODUCTION

Nanocomposite materials have been extensively investigated in bulk and thin film forms because of their wide range of applications, starting from traditional industries as general mechanics and automobiles, paper mills, textiles, food industries to high tech industries such as microelectronics and magnetoelectronics [1]. Nanocomposites acquire synergistic properties of its matrix and the guest material. According to the nature of matrices, nanocomposites can be classified into three main categories i.e. metal-matrix, ceramic-matrix and polymer-matrix nanocomposites [2].

Various techniques have been considered to prepare nanocomposite materials including thermal, plasma spraying and physical and chemical vapor deposition [3]. Among these methods that is widely used, electrodeposition which offers several advantages when compared with other techniques including precise control, low energy requirements, uniform deposition, low cost in production of large area samples, good reproducibility, versatility, capability to coat complex component geometries, high production rate and reduction of waste [4,5].

In particular nickel deposits prepared by electrodeposition is characterized by its high density, minimum porosity, excellent corrosion resistance and good wear resistance [6] and the reduction in the grain size of Ni deposit leads to increase of the strength and strain hardening rate [7]. For nickel matrix electrodeposits, a great variety of particles have been used such as oxides i.e. TiO_2, SiO_2, Al_2O_3, CeO_2, ZrO_2, SnO_2 and Cr_2O_3 [8-13], carbides like WC [14], TiC [3] and SiC [1,15-19], nitrides like Si_3N_4 and BN [20-22], carbon nanotubes [23], etc.

Several parameters can influence the electrodeposition process and consequently the microstructure of the composite coating, these parameters include: the electrolysis conditions (composition of the electrolyte bath, presence of additives, pH, temperature and electrolyte agitation), current conditions (type of imposed current and values of current density) and the properties of the reinforcing particles (size, surface properties, concentration and type of dispersion in the bath).

In this review, general aspects related to the mechanisms of electrodeposition, different parameters affecting the process of Ni ceramic nanocomposites will be discussed. The article will throw light on the effects of these parameters on the microstructure, physical and mechanical properties of the coatings and different techniques that can be used in characterization of the composite coatings.

2. THEORETICAL MODELS OF METAL-MATRIX COMPOSITE ELECTRODEPOSITION

The process of particle incorporation in the metal matrix during electrocodeposition may be described through the following steps:
1. Particles transfer from the bulk of the solution to the metal surface
2. Interaction i.e. adsorption of particles with the electrode surface
3. Particle embedding in the growing metal matrix

The first model that accounts for the electrodeposition of metal reinforced with particles was proposed by Guglielmi [24]. According to this mechanism the electrocodeposition process proceeds via two steps. Firstly, particles are weakly adsorbed on the cathode surface by Van der Waals forces with high degree of surface coverage which can be presented by Langmuir adsorption isotherm. Secondly, particles are strongly adsorbed on the surface by Coulomb forces under the effect of applied electric field and incorporated in the growing metal matrix. According to this model the volume fraction of the incorporated particles, α, can be expressed as:

$$\frac{\alpha}{1-\alpha} = \frac{zF\rho_m V_o}{M_m i_o} \cdot e^{(B-A)\eta} \cdot \frac{kc_b}{kc_b+1} \tag{1}$$

where M_m and ρ_m are the atomic weight and the density of the deposited metal, respectively, i_o is the exchange current density, z is the valence of the electrodeposited metal, F is Faraday constant, η is the electrode overpotential, c_b is the bulk concentration of particles and k is the Langmuir adsorption constant. The main drawback of this model is that it neglects the particle size, hydrodynamics i.e. mass transfer of particles.

Celis [25] proposed a five-step mechanism to account for the electrocodeposition process: (1) formation of ionic cloud around the particles; (2) mass transfer of particles by convection to the hydrodynamic boundary layer; (3) mass transfer of particles to the cathode surface by diffusion; (4) adsorption of free ions and electroactive ions adsorbed on the particles on the cathode, and (5) electroreduction of adsorbed ions accompanied with incorporation of particles into the growing metal matrix.

According to Kurozaki study [26], dispersed particles are transferred to the Helmholtz's double layer by mechanical agitation in the first step. Secondly, particles which are charged in the high potential gradient are transferred to cathode by electrophoresis. In the third step, particles are adsorbed on the cathode surface by coulomb attraction between them and adsorbed anions on the cathode and hence are incorporated into the growing metal layer. Other models were suggested by authors [27,28] but still more work is needed that accounts more with the particle characteristics (composition, size, crystallinity, …) and the operating electrodeposition parameters.

3. PARAMETERS AFFECTING THE ELECTRODEPOSITION PROCESS
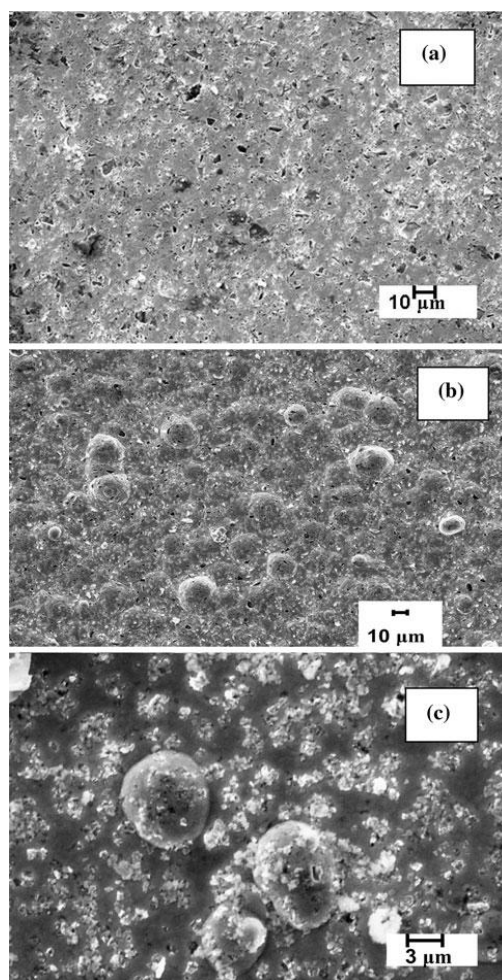
3.1. Effect of particle characteristics

Figure 1. SEM images of: (a) Ni-Al$_2$O$_3$-1, (b) Ni-Al$_2$O$_3$-2 and (c) Ni-Al$_2$O$_3$-3 [30]

It is well known that the electrode/particle interaction depends to a great extent on the particle properties (type, size, shape, surface charge, concentration and dispersion in the bath). Generally, the codeposition of nano-sized particles produces a composite coating with a much higher hardness than achieved with micron-sized particles [5]. The smaller the particle, the greater the effect of colloidal properties (Van der Waals, electrostatic and solvent interaction forces). It should also be noticed that the smaller the particle size is, the more difficult the codeposition into the metal matrix due to high tendency of agglomeration [29].

S.T. Aruna et al [30] studied the synthesis and characterization of Ni-Alumina composite coating using different phases of alumina i.e. α-Al_2O_3 (Al_2O_3-1), γ-Al_2O_3 (Al_2O_3-2) and commercial alumina (Al_2O_3-3 containing mixture of α-, δ- and γ-phases). They observed that there was a change in the microstructure of the coating depending on the phase type. Only nodular microstructure was obtained when γ-Al_2O_3 was used, on the other hand the microstructure obtained on using commercial Al_2O_3 exhibited a mixture of nodular and smooth surface (Figure 1). The study also indicated that the Ni grain sizes as calculated from Scherrer formula were 25, 16 and 11 nm for Ni-Al_2O_3-1, Ni-Al_2O_3-2 and Ni-Al_2O_3-3, respectively.

The zeta potential which is a measure of the particle surface charge represents an indication to the stability of the colloidal particles. This means that higher zeta potential induces lower susceptibility to agglomeration i.e. higher concentration of non-agglomerated particles in the solution which is very essential for incorporation of the particles into the growing metal matrix during the electrocodeposition process. The zeta potential is affected by several parameters such as pH, ionic strength, concentration of the particles in the solution and type of counter ions...etc. At pH values lower than the point of zero charge the particles are positively charged and hence it is expected to be electrostatically attracted to the cathode by migration i.e. can be imbedded into the metal matrix. On the other hand, at higher pH values than the point of zero charge the particles are negatively charged and it is expected to be repelled from the cathode. Nevertheless, some studies indicated that even negatively charged particles can be incorporated into the growing metal on the cathode surface [31]. This was attributed to the absolute value of the zeta potential is also a key factor and not only its polarity.

3.2. Effect of temperature

The effect of temperature on the microstructure of the electrodeposited coating was investigated by many researchers [32-34]. The effect of temperature on the percent of SiC codeposition into Ni matrix was studied by Vaezi et al [35]. Their results showed that the percent of codeposited SiC nanoparticles increases with temperature of the plating bath up to 50 ºC. This behavior was attributed to increase of activity of SiC particles with temperature. However, at higher temperatures the cathode overpotential decreased and hence the adsorpability of the particulates which decreased the percent of their incorporation in the metal matrix.

The influence of bath temperature on the volume percent of TiCN in the Ni-TiCN nanocomposite formed by electrocodeposition was also studied [36]. It was observed that the percent of embedded TiCN in the nanocomposite increased with increasing the bath temperature up to 50 ºC

but above this temperature range a decreasing trend was observed which was attributed to the decrease in the current efficiency of deposition at high temperature (Figure 2).
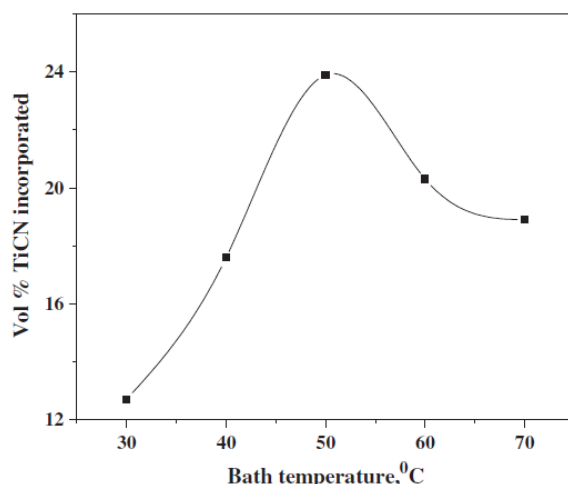

Figure 2. Effect of bath temperature on vol.% incorporation of TiCN in the Ni–TiCN composite deposit obtained at 6 g l^{-1} TiCN particle concentration at pH 4 and 4 A dm^{-2} [36].
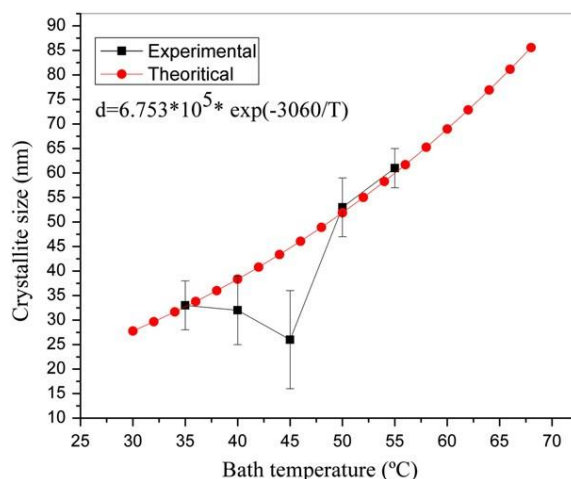

Figure 3. The effect of temperature on the crystallite size of Ni in Ni-CeO$_2$ nanocomposite [37]. A comparison between experimental data and theoretical curve

R. Sen et al [37] deduced the following relation between the average grain size in Ni-CeO$_2$ nanocomposite coating and the bath temperature:

$$d = 6.753 x 10^5 \exp\left(\frac{-3060}{T}\right)$$ (2)

According to equation 2, it was expected that the grain size increases with the bath temperature, however, a contrary behavior was observed where the crystallite size of Ni decreased with an increase in the bath temperature up to 45 ºC (Figure 3). This discrepancy was attributed to the two contradictory effects of temperature increase on the thermodynamic and kinetic driving force [38]. As the temperature increases, the thermodynamic driving force of crystallization decreases with an increase in the critical size of the nucleus resulting to lower nucleus densities i.e. formation of coarse grain

[33,39]. On the other hand, the increase in temperature leads to increase in the kinetic driving force which leads to increase in the rate of nucleation and subsequent formation of fine grains [38]. Hence, it was concluded that below 45 ℃ the kinetic driving force is the dominant factor in determining the crystallite size, whereas above 45 ℃ the thermodynamic driving force is the controlling factor of the nucleation rate.
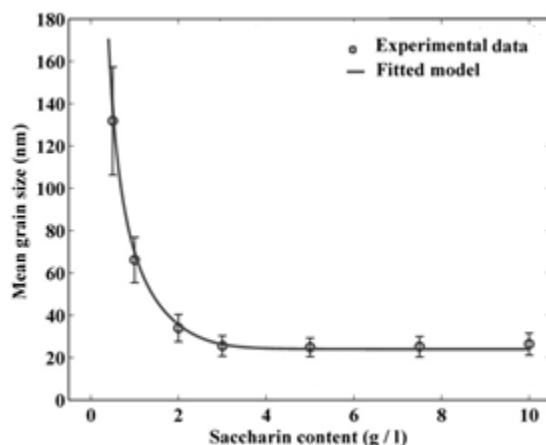
3.3. Effect of additives

Figure 4. Effect of saccharin concentration in the plating bath on the grain size of Ni [38]. Comparison of experimental data and theoretical model.

Many studies reported the effect of additives in the plating bath on the microstructure and physical properties of Ni deposits. It was found that the addition of saccharin to Ni plating bath improve the ductility, brightness and in addition it acts as a grain refiner agent. The role of additives as a grain refiner can be summarized as: (i) blocking the surface by complexation, decreasing the diffusion of adsorbed Ni ions on cathode so retards the crystal growth [40-44], (ii) affecting the rate of hydrogen evolution on cathode, (iii) changing the cathodic overpotential [45,46].

Amadeh et al [38] studied the effect of saccharin concentration on the average grain size of Ni deposits (Figure 4). They derived a simple model of the relationship between saccharin concentration and average grain size of Ni deposits by considering Langmuir adsorption mechanism and general relationship the average grain size of deposit and true current density of reduction and they deuce the following relation:

$$\bar{d} = k_s(1 + kC_s^m)^{n'} \tag{3}$$

where $\bar{d}$ is the average grain size of deposit, C_s is the bulk concentration of additive, k, m, n′ and k_s are constants. From non-linear curve fitting to experimental data, the following numerical relationships were obtained:

$$\bar{d} = 24(1 + 2000C_s^{-7})^{0.14} \tag{4}$$
$$\bar{d} = 15(1 + 2000C_s^{-7})^{0.09} \tag{5}$$

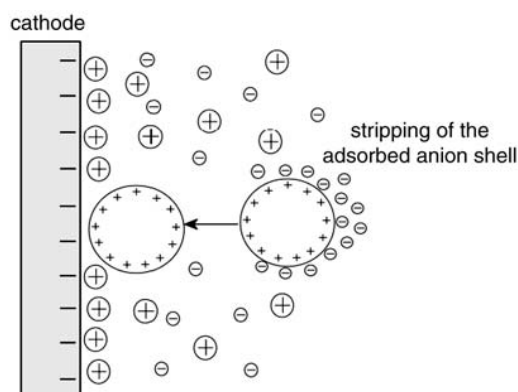*3.4. Effect of bath composition and pH*

Figure 5. Schematic representation of the charge distribution during the electrodeposition of nanoparticles [48]
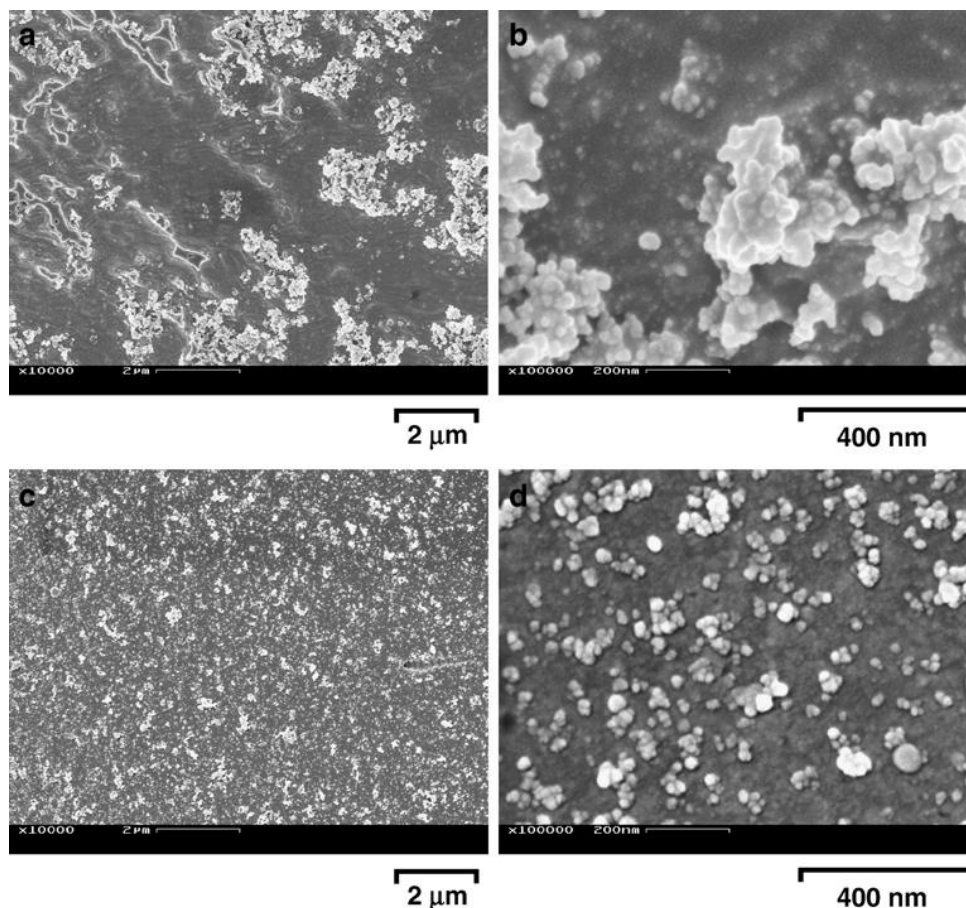

Figure 6. Cross sectional scanning electron micrographs of nickel composite coatings; (a,b) acidic sulfamate bath; (c,d) alkaline pyrophosphate bath [47].

Nickel/alumina nanocomposites coatings were electrodeposited on copper cathode from an acidic sulfamate bath (pH = 4.3) and alkaline bath containing pyrophosphate as a complexing agent (pH = 9.5) [47]. Significant higher alumina content in the layers deposited from alkaline pyrophosphate solution compared with acidic electrolyte was observed. This was explained on the fact that the surface charge of the particles plays a significant role in the electrocodeposition process [48].

In the alkaline deposit, alumina particles acquire negative charge due to specific adsorption of citrate and pyrophosphate anions. During the electroplating process, the electrode bears negative excess charge and its electrolytic part of its double layer acquires increased concentration of positive excess charges. Although the particles have electrical double layers around them but they are deformed during movement of particles towards the electrode. When these particles enter the electrical double layer of the electrode, the shell of specifically adsorbed anions will be stripped off and particles are included in the growing metal matrix [49] (Figure 5).

It was also observed that the distribution of alumina particles in nickel matrix deposited from acidic sulfamate bath was non-unifrom and the codeposited particles appear as agglomerates, whereas the deposition in alkaline pyrophosphate solution showed a homogeneous distribution of particles within the metal matrix and particles were incorporated in much smaller agglomerates within the range of 100 nm (Figure 6).

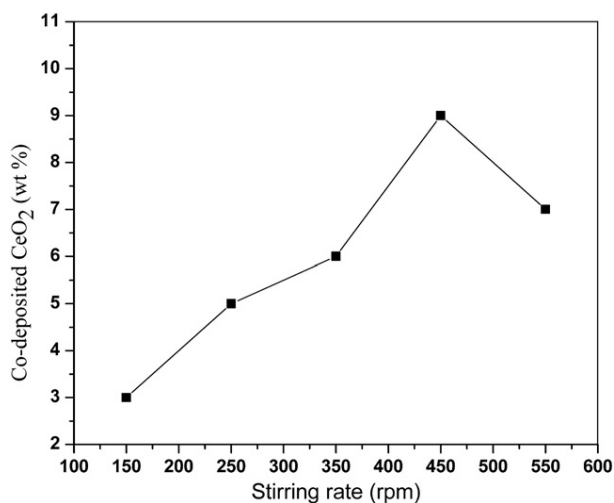### 3.5. Effect of bath agitation and rotational speed

Figure 7. Effect of stirring rate on the amount of ceria in the composite coating [54].

The main purpose of agitation during electrocodeposition of dispersoids within metal matrix is to keep the particles suspended and prevent their sedimentation or floating. The rate of stirring affects the co-deposition has two contradictory ways i.e. (i) increasing the rate of agitation leads to increase the content of particles in the nanocomposites [50], (ii) at high rates of agitation the particle nanocomposites content decreases [51]. In addition, the mean size of incorporated particles in the metal matrix decreases rapidly because large particles are removed easily.

Vaezi et al [52] investigated the effect of stirring rate on the Ni/SiC composite and reported that increasing the stirring rate up to 120 rpm causes increase the SiC percent decrease due to collision factor. The same trend was observed by Baghery et al [53] in the electrodeposition of Ni/TiO$_2$ nanocomposite.

Ranjan sen et al [54] also studied the effect of stirring rate on the microstructure of Ni/CeO$_2$ nanocomposite. It was observed that the amount of codeposited CeO$_2$ particles increases up to stirring

rate of 450 rpm whereas at higher stirring rates the incorporation of CeO_2 decreases as a result of collision factor and also due to increasing streaming velocity of the suspension sweep away loosely adsorbed CeO_2 nanoparticles from the cathode surface making the rate of particles removal higher than the rate of attachment so decreases the amount of codeposited CeO_2 in the nanocomposites coating (Figure 7).
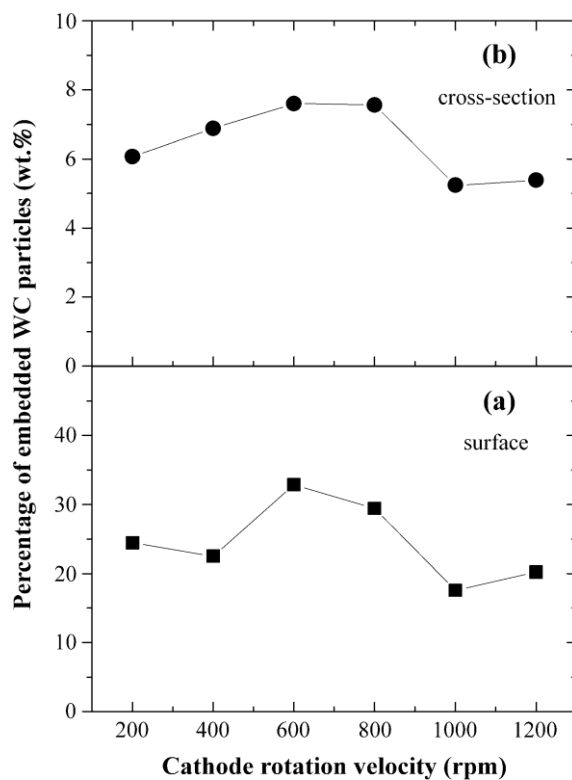

Figure 8. Dependence of percentage of embedded WC particles (a) on the surface and (b) on the cross-section of the composite coatings [14].

Electrocodeposition of ultrafine WC into Ni matrix was studied on a rotating disk electrode with various rotation velocities (ω) in the range of 200-1200 rpm under pulse and direct current conditions [14]. This study revealed that as the rotation velocity was increased, the incorporation of particle into the composite increased up to certain limit. On the other hand, at very high rotation velocities the codeposition percentage tended to decrease which was attributed to removal of the attached particles before embedding into the metal matrix due to intense radial flow (Figure 8).

The agglomeration of particles in the plating bath can also be reduced by ultrasonic energy treatment. The propagation of ultrasound waves in the solution generates large pressure causing stress that destroy the binding energy between particles. Kuo et al [55] studied the effect of ultrasound energy on the electrocodeposition of Ni-alumina composite coating. They reported that the diameter of the agglomerated alumina particles could be reduced by applying ultrasound energy but the resulting dispersion is limited which led to low alumina content within the composite coating. The alumina content can be increased by decreasing the concentration of Ni^{2+} ions in the plating bath.

3.6. Effect of surfactant

It was reported by many researchers that addition of a cationic surfactant increases the particle co-deposition in the metal matrix [56,57]. The enhancement of particle codeposition into metal matrix is associated with the modifications take place on the particle surface caused by adsorbed ions or surfactant molecules. This adsorption promotes the electrophoretic migration of the particle towards cathode but this effect is more pronounced if the particle size is in nanoscale [58].
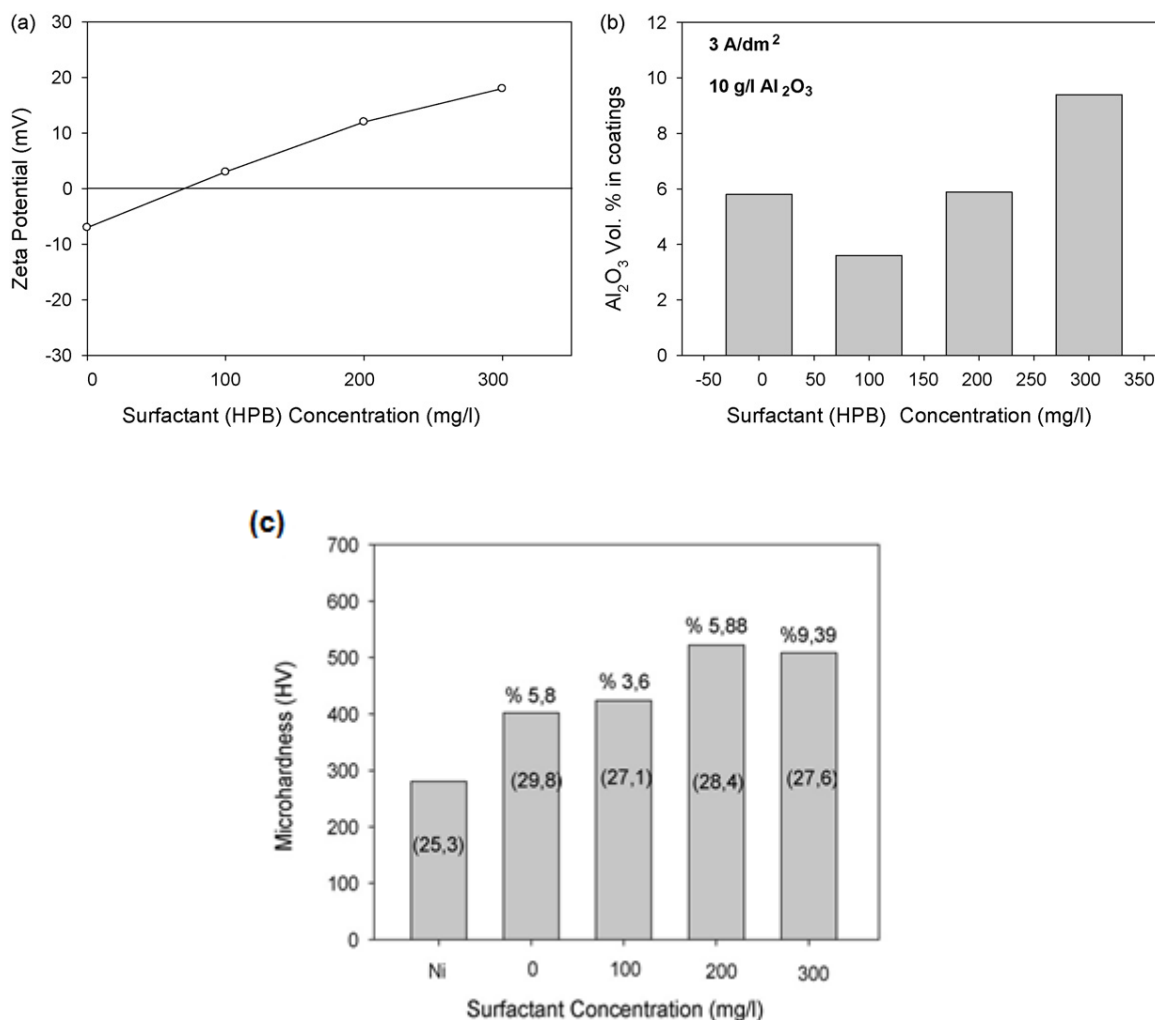
Figure 9. The effect of surfactant (HPB) concentration on the: (a) zeta potential (b) volume percentage of co-deposited Al_2O_3 particles (c) microhardness [64]

The cationic surfactant can adsorb on the particle surface developing a net positive charge on its surface so increasing their affinity towards cathode and hence increases the stability of particles suspension and prevents agglomeration. In this way it is believed that cationic surfactant enhances the incorporation of particles in the metal matrix. However, the extent of particles co-deposition depends on the type of surfactant. The use of oleyl dimethyl amine oxide surfactant yields a maximum SiC content 48 vol % in Ni matrix [59]. The SiC content rises to 50 vol % when a fluorocarbon surfactant

was used [60,61].   When azo-cationic surfactant containing an ethyl group was used the co-deposition of SiC particles was enhanced to 62.4 vol % [62].

The effect of cetyltrimethyl ammonium bromide (CTAB) on the co-deposition of SiC in Ni matrix was investigated [63]. The addition of CTAB promoted the uniformity of distribution of SiC particles in the co-deposition layer and increasing its concentration allowed larger particles to be imbedded in the co-deposit, i.e. the effective size of particles was shifted to higher values.

Gül et al studied the effect of hexadecyl pyridinium bromide (HPB) on the co-deposition of Ni-alumina nanocomposite coating [64]. It was observed that the vol % of alumina in the composite coating increases with increasing the amount of HPB starting from certain concentration (200 mg/l). Below this concentration the zeta potential of the surfactant is very close to 0 mV, few amount of nano-alumina particles were co-deposited and significant segregation take place (Figure 9a and b). It was also observed there is an increasing trend of the microhardness, grain size and friction coefficient of Ni-Al$_2$O$_3$ nanocomposite till a maximum at certain concentration of HPB (200 mg/l) after which tested parameters decreased (Figure 9c).

$$H_{2n+1}C_n{-}\!\!\left\langle\bigcirc\right\rangle\!\!{-}N{=}N{-}\!\!\left\langle\bigcirc\right\rangle\!\!{-}O{-}C_2H_4{-}\overset{+}{N}(CH_3)_3\,,\ \overset{-}{Br}$$
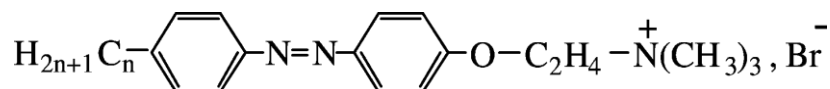
Figure 10. Molecular structure of AZTAB. Where, n = 0, C0-AZTAB [azobenz-ene-4t-(oxyethyl) trimethyl ammonium   bromide], n = 2, C2-AZTAB [4-ethyl-azobenzene-4t -(oxyethyl) trimethylammonium   bromide], and n = 4, C4-AZTAB [4-butylazobenzene-4t -(oxyethyl) trimethyl ammonium bromide] [65].
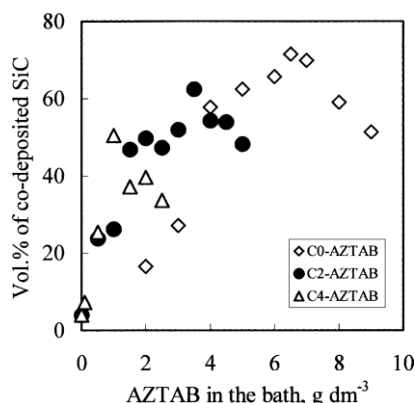

Figure 11. Effect of AZTAB on the extent of co-deposition of SiC into Ni-SiC composites coating [65].

The influence of the hydrophobic chain length of a cationic surfactant, azobenzene-4′-(oxyethyl)trimethyl ammonium bromide (AZTAB) derivatives (Figure 10) on the co-deposition of SiC particles in Ni matrix was studied [65]. It was observed that the surfactant with shortest tail deposit the highest amount of SiC particles. There was an increase in the particle co-deposition for the increase in the AZTAB but to a certain limit beyond which a decreasing trend of particle co-deposition was observed. The maximum amount of co-deposited SiC was taking the order of C0-AZTAB > C2-

AZTAB > C4-AZTAB which was attributed to the difference in the rate of AZTAB desorption from the particle surface near the cathode before deposition (Figure 11).

3.7. Effect of ceramic concentration

The dependence of particle content in the deposit and consequently the microstructure and coat properties on the particle content in the plating bath was studied by many authors [3,36]. In all studies the vol % of the codeposited particles in the coatings, irrespective the particle size, with increasing the concentration of the particles in the plating solution up to a certain limit the remains constant or decreased. Ramesh Bapu et al investigated the extent of TiCN incorporation into Ni matrix with respect to TiCN concentration in the plating bath [36]. It was observed that irrespective to the value of applied current density, the particles incorporation in the metal matrix increases to a certain maximum limit but decreased after further addition of TiCN in the plating bath (Figure 12).
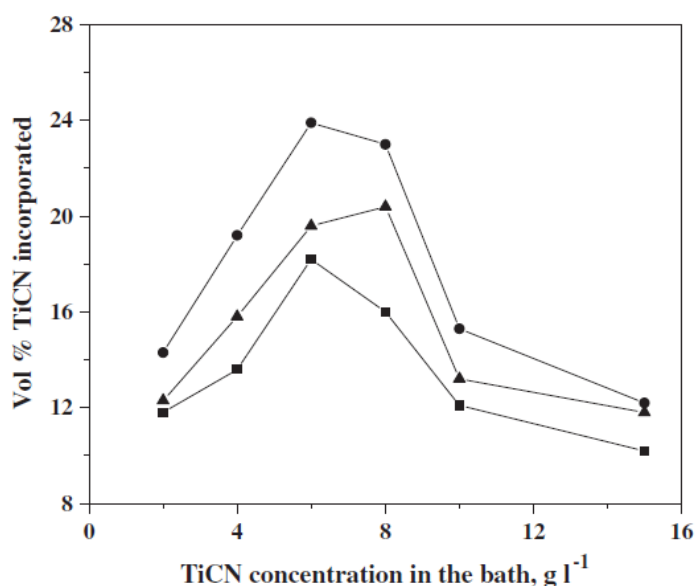

Figure 12. Effect of TiCN concentration in the bath and current density on vol.% incorporation of TiCN in the Ni–TiCN composite deposit at pH 4 and 50 °C. ■–■–■– 2 A dm^{-2}, ●–●–●– 4 A dm^{-2}, ▲–▲–▲– 10 A dm^{-2} [36].

3.8. Effect of solvent

Some studies involving the electrocodeposition of metal matrix composites in non-aqueous electrolytes were performed [66]. Water can be substituted partially or completely with organic solvents to avoid hydrogen embrittlement, to improve the wettability of the electrode and to realize a wide electrochemical window [67]. It was found that hydrophilic particles that cannot be deposited from aqueous solution, can be easily deposited into aluminum matrix from organic electrolytes [68,69]. Shrestha et al studied the codeposition of Ni-ceramic composite in ethanol based nickel bath [70]. The maximum amount of particle codeposition in the Ni matrix was observed in pure ethanol. In

addition, the anti-wear performance of the composite coatings obtained in ethanol based electrolyte is better than those obtained from Watts plating bath. Ni-TiO$_2$ composite and nanocomposite coatings were prepared in mixed aqueous-organic solvent i.e. aqueous electrolyte containing 50% diethanol amine [71]. It was observed that no significant varaiation in the particle content of coatings on using sub-micron or nanosized TiO$_2$ particles which means that gravitational forces and diffusion have no considerable influence on the electrocodeposition process in this electrolyte.

Singh et al investigated the electrocodeposition of Ni-TiC composite in acetate bath using N-methyl formamide as non-aqueous solvent [3]. They investigated the composition, microstructure, hydrogen content and microhardness. They reported that almost hydrogen-free deposit could be obtained with improved microhardness value.

3.9. Effect of magnetic field

Over the past decades, several authors investigated the effect of magnetic field on the electrodeposition of metals and alloys [72-76]. Both the intensity and the direction of the imposed magnetic field affect the properties of the deposit. Yamada et al [77] studied the electrodeposition of Ni-Al$_2$O$_3$ composite in vertical magnetic field and they found that Al$_2$O$_3$ particles were included in the matrix in a regular manner. The application of high magnetic field was used instead of mechanical agitation and successfully produced Ni-Al$_2$O$_3$ nanocomposite [78]. The amount of nano-Al$_2$O$_3$ particles in the composite coating increased with increasing the magnetic flux density and reached maximum at 8 T, then slightly decreased. This increase in the amount of incorporated Al$_2$O$_3$ partricles was accompanied with significant enhancement in the hardness and the wear resistance. Application of parallel superimposed magnetic field on the electrocodeposition process of Ni-Al$_2$O$_3$ nanocomposite coating improved the current density and produced network shaped nanoparticles distribution [79].

It is well-known that application of magnetic field can enhance the mass transfer in the electrochemical reactions which is known as magnetic hydrodynamic effect [80]. The magnetic force is expressed as Lorentz force density which induces the motion of the fluid and consequently enhances the mass transport [81]:

$$f_L = j \times B \tag{6}$$

where j is the current density and B is the magnetic flux density. According to equation 6 the magnetic nanoparticles will move in the electrolyte towards regions with higher magnetic flux due to magnetophoretic force (f_{mp}):

$$f_{mp} = \frac{\Delta x}{\mu_o}(B.\Delta B) \tag{7}$$

Where x is the susceptibility of the particles and μ_o is the magnetic permeability of the free space. f_L acts on the fluid whereas f_{mp} acts on the particles. The circulation velocity is proportional to the intensity of magnetic flux. The circulation produced by Lorentz force is more effective in particle incorporation when compared with mechanical agitation.

3.10. Effect of current density

Generally, the amount of particles incorporation in the metal matrix is enhanced by increasing of the current density up to a limit and beyond this value the nanoparticles content in the coating decreased. It was suggested that the particles adsorbed cations moved directly to the cathode under the effect of gravitational force and electronic force then captured by the growing metals. At low current densities the rate of transfer of particles is faster than the growth rate of the metal. On the other hand, at higher current densities the situation is reversed so the particle content in the composite coating decreases [79]. Gul et al [64] observed the same behavior in the electrocodeposition of Ni-alumina composite. They suggested that the maximum in the volume percent of alumina is due to transition from activation-controlled metal deposition to a diffusion-controlled process.
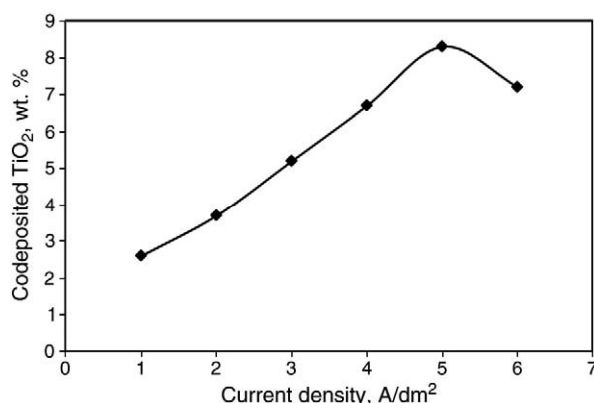

Figure 13. Variation of wt.% of codeposited TiO_2 vs. the current density (TiO_2 concentration in bath=30 g/l, T=50°C, stirring rate=180 rpm) [82].

A similar behavior for the dependence of the wt. % of particles in the coating on the current density for Ni-TiO_2 composite was observed [82]. It was suggested that at current density less than 5 A/dm^2, the increase in the particles content with current is due to increasing the rate of arrival of adsorbed nanoparticles to the cathode surface. At higher current densities, the rate of movement of metal ions becomes faster than the adsorbed nanoparticles so rapid reduction of the metal ions at the cathode surface decreases the TiO_2 content in the coating (Figure 13).

3.11. Type of current

It is well known that pulse electrodeposition technique permits greater control in the properties of the deposits and greatly improves their microstructure. It was reported that the use of pulse current causes significant reduction in the internal stress of the deposited articles when compared to conventional direct current with the same average current density [83,84]. Yang et al [85] found that Ni coatings produced by pulse plating techniques have less porosity and higher corrosion resistance compared to those obtained by direct current. In case of Ni/SiC codeposits, the use of pulse current technique results in production of coatings with higher percentage of particles incorporation, reduced

grain size, lower friction coefficient with nano SiC reinforcement, higher microhardness and more uniform distribution of SiC particles within the Ni matrix than coatings obtained by direct current [86-91].

In pulse electrodeposition technique the potential or current is alternated between two different values which results in a series of pulses of equal amplitude and separated by zero current (Figure 14). In such way each pulse consists of an on-time (t_{on}) i.e. during which current is applied and an off-time (t_{off}) i.e. during which no current is applied. If the pulse height is i_P, the average current density $\bar{\iota}_A$ can be defined as:

$$\bar{\iota}_A = \frac{(i_P.t_{on})}{(t_{on}+t_{off})} \tag{8}$$

The duty cycle is the ratio of pulse length (on-time) to the sum of on- and off-time and the frequency is the reciprocal of the sum of t_{on} and t_{off}.

$$duty\ cycle = \frac{t_{on}}{t_{on}+t_{off}} \tag{9}$$

$$frequency\ (f) = \frac{1}{t_{on}+t_{off}} \tag{10}$$

$$\bar{\iota}_A = i_p x\ duty\ cycle \tag{11}$$

During the on-time ions are depleted near the cathode and ions migrate to the interfacial region when the current is off and the cycle is repeated.
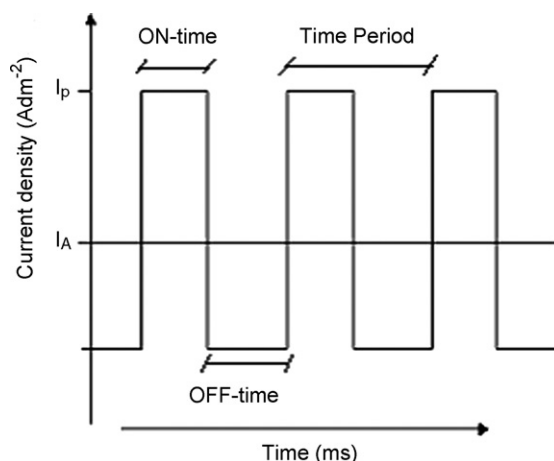

Figure 14. Typical pulse-current waveform.

In the pulse-reverse technique (PRC) a stripping time is introduced into the plating cycle, during which the metal surface protrusions selectively dissolves, which results in more uniform deposit (Figure 15). PRC technique has several advantages compared to PC technique e.g. the amount of nanoparticles incorporated in metal deposit can be enhanced, lower concentrations of nanoparticles in the plating bath can be used, and selective incorporation of similar size nanoparticles take place.
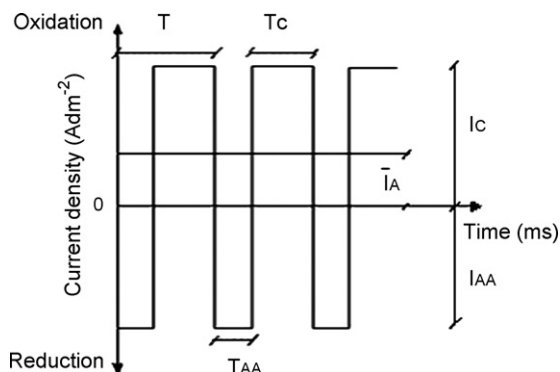
Figure 15. A typical pulse reverse waveform where, T_{AA} is the anodic time, T_C is the cathodic time, I_{AA} is the anodic current density, I_C is the cathodic current density, $\bar{I}_A$ is the average current density, T is the cycle time.

3.11.1. Effect of duty cycle

The effect of duty cycle on the properties of composites prepared by electrocodeposition was the subject of interest by many authors. Guo *et al* [92] studied the effect of duty cycle on the properties of rare earth-Ni-W-P-SiC composite coating. They reported that at the same pulse frequency, the microhardness increased with increasing the duty cycle. Sen *et al* [93] investigated the effect of duty cycle on the microstructure and microhardness of pulse electrodeposited Ni-CeO$_2$ nanocomposite coating. The thickness of the sample increased with increasing the duty cycle, whereas the crystallite size changes from micro scale to the nano scale as the duty cycle increased and the microhardness of the nanocomposite increased with increasing the duty cycle (Figure 16).
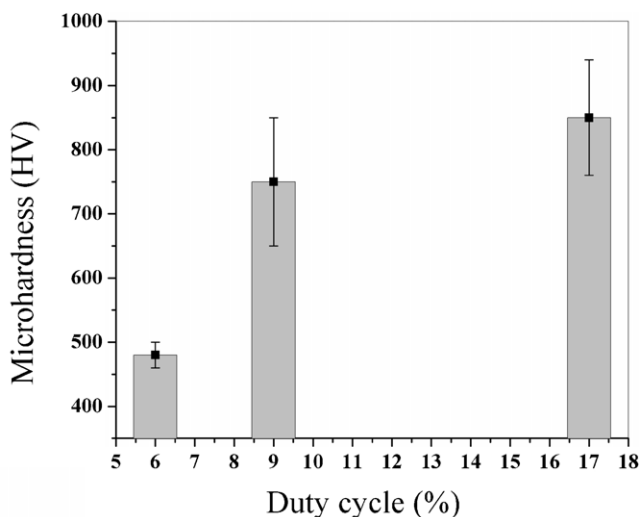

Figure 16. Microhardness of Ni–CeO$_2$ nanocomposite coating deposited with different duty cycles: (a) 6%, (b) 9% and (c) 17% [93].

For Ni-alumina nanocomposite coating, it was observed that lower duty cycles led to increase of the vol % of alumina in the composite (Figure 17). This observation was attributed to that at longer

pulse-off-time, more Al_2O_3 particles which carry adsorbed Ni ions, reach the cathode by convection and diffusion. In the subsequent pulse-on-time, the ions adsorbed on the particles will be discharged and the particles are incorporated in the growing metal layer [94].
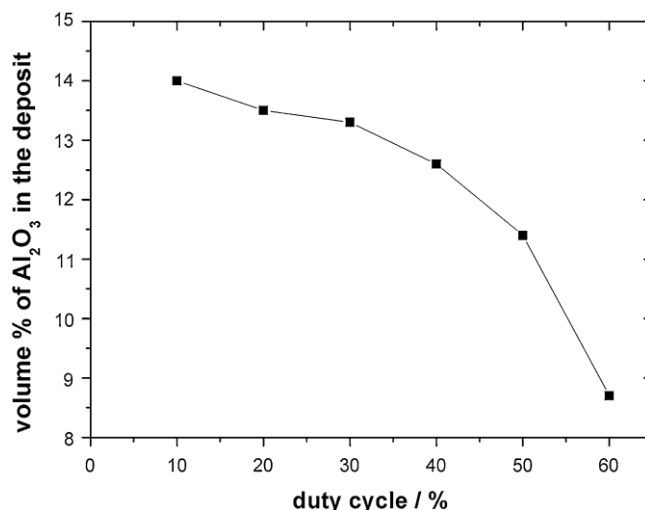

Figure 17. Effect of pulse duty cycle on the alumina content of the composite [94].

From their study on the electrocodeposition of Ni-alumina composite, Bahrololoom *et al* [95] found that the composite coatings electrodeposited at low duty cycles contain higher percent of embedded alumina and higher proportion of large size particles, whereas those deposited at high duty cycles have lower percent of incorporated alumina and particles have smaller size (Figure 18). This behavior was attributed to the fact that as the pulse off-time increases (low duty cycles) large particles can reach the cathode due to mass transfer. On the other hand at high duty cycles i.e. short off-times, only particles of small size can reach the cathode surface and incorporated into the growing metal matrix.
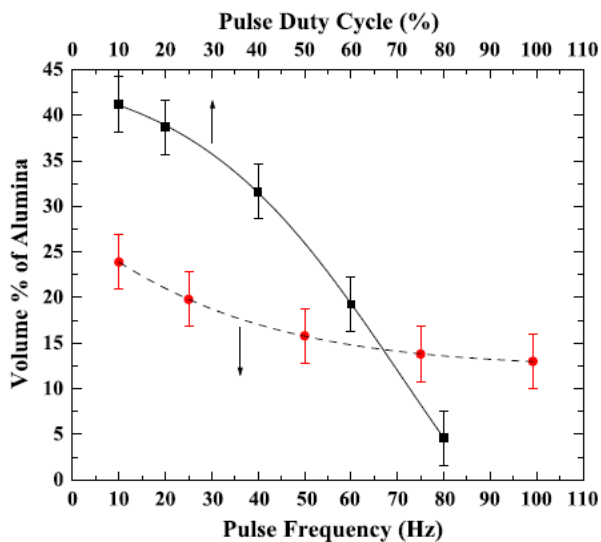

Figure 18. Effect of pulse duty cycles with 50 Hz frequency (solid line) and pulse frequency with 60% duty cycle (dash line) on the alumina content of nickel–alumina composite coatings electrodeposited with a pulse current of 5 A dm^{-2} [95].

3.11.2. Effect of pulse frequency

The percent inclusion of particles in metal ceramic nanocomposite prepared by pulse electrocodeposition and in consequence the microstructure, hardness and other mechanical properties of the composite coatings is affected by the pulse frequency. Generally, the percent of the particles in the composite increases gradually with increasing the pulse frequency to certain limit regardless the value of imposed current density. The pulse frequency effects on the properties of nickel matrix composite coatings reinforced with sub-microsized Al_2O_3 particles ($Ni–Al_2O_3$) were investigated [96]. The results showed that the pulse frequency significantly influenced the preferred orientation of $Ni–Al_2O_3$ composite coatings; the texture of the coatings progressively changed from a strong (111) preferred orientation to a random orientation when pulse frequency increased (Figure 19).
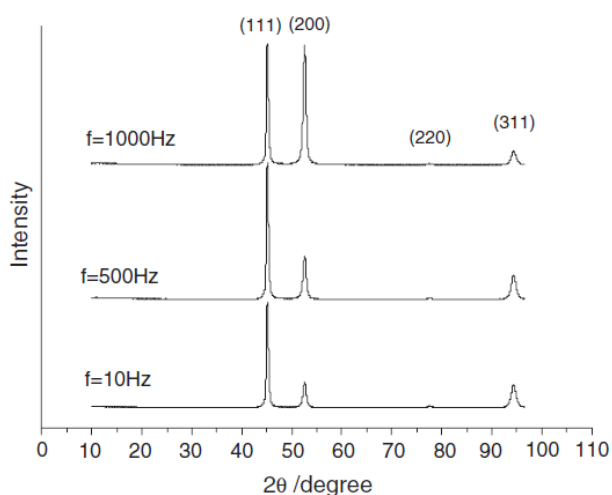

Figure 19. The effect of pulse frequency on the XRD peaks of $Ni–Al_2O_3$ composite coatings [96].

4. CHARACTERIZATION TECHNIQUES OF NANOCOMPOSITE COATINGS

Several techniques are used to study the morphological, electrochemical, physical and mechanical properties of the coating including SEM-EDX, Microhardness measurement, X-ray diffraction (XRD), transmission electron microscopy (TEM), X-ray photoelectron spectroscopy (XPS), atomic force microscopy (AFM), wear resistance, electrochemical impedance spectroscopy (EIS) and electrochemical polarization…etc.

In order to determine the amount of codeposited particles into the composite coating, the density of the composite can be determined using helium pycnometry due to significant difference in density between pure Ni and Ni-ceramic nanocomposite. This technique has advantages over other gravimetric methods in that it is non-destructive method and does not need special sample geometry. The volume fraction ϕ of particles in the composite can be evaluated according to equation 12:

$$\emptyset = \frac{\rho_s - \rho_{matrix}}{\rho_{particle} - \rho_{matrix}} \qquad (12)$$

where ρ_s is the measured density of the specimen and ρ_{matrix} and $\rho_{particle}$ are the standard values of densities of the Ni matrix and dispersed particles, respectively [94].

The weight percent of incorporated particles into the metal matrix can also be determined using EDX analysis [47]. This analysis can be performed both on the surface and in the cross section but this method is not so accurate so its application is limited to semi-quantitative analysis.

The weight percent of incorporated particles into the metal matrix can be also estimated by determining the weight of the coating before and after the electrocodeposition process. The coating is then peeled off, dissolved and analyzed using atomic-absorption spectrometry or ICP technique.

XRD is an essential technique in characterization of the composites which can be used to determine the crystallite size and lattice strain using Cu Kα radiation. The crystallite size can be obtained using modified Williamson-Hall method [97,98]. In this method it is assumed that the X-ray diffraction peak is a convolution of Lorentzian curve (influence of the grain size) and Gaussian curve (broadening due to strain). Depending on this assumption, the relation between the integral breadth (β), average crystallite size (D) and the lattice strain (ε) can be expressed as follows:

$$\frac{\beta \cos\theta}{\lambda} = \frac{1}{D} + 2\varepsilon \left(\frac{2\sin\theta}{\lambda}\right) \tag{13}$$

$$\text{or } \Delta K = \frac{1}{D} + 2\varepsilon K \tag{14}$$

the plot of ΔK versus K gives the values of the crystallite size (from the intercept) and the strain (from the slope).

The broadening of the peaks in the XRD patterns is usually attributed to three factors, i.e. instrumental error, lattice strain and nano-sized crystallite [93]. Before analyzing the XRD pattern it is important to separate the overlapping peak. In order to make this several mathematical methods are used to find the hidden peaks. The preferred crystalline orientation of the deposits and its quality can be estimated using the term Relative Texture Coefficient (T_c) which is defined as:

$$RTC_{(hkl)} = \frac{I_{s(hkl)}/I_{p(hkl)}}{\sum_{i=1}^{6} I_{s(hkl)}/I_{p(hkl)}} \times 100 \tag{15}$$

where $I_{s(hkl)}$ and $I_{p(hkl)}$ are the diffraction intensities of the (hkl) plane measured in the diffractogram of the deposit and the standard Ni powder sample, respectively. For Ni only the six basic lines of the total reflection lines are considered, i.e. (111), (200), (220), (311), (331) and (420) because the diffraction lines (222) and (400) are second-order diffractions of (111) and (200) planes, respectively. The $RTC_{(hkl)}$ refers to the relative intensity of a given orientation with respect to the 6 orientations in the Ni or Ni composite coating. The preferred orientation of a plane is indicated by values of RTC greater than 16.67 % [99].

DIRECT CURRENT AND RADIOFREQUENCY GLOW DISCHARGE

When coupled to optical emission spectrometry (OES) or mass spectrometry (MS) can be used surface analysis based on the advantages of being used in depth profile analysis with high depth resolution, low detection limits, low cost and reduced matrix effects. In dc-GDs [100] a potential breaks the discharge gas (high purity argon gas) in a low pressure chamber yielding argon ions which

are attracted to the sample. The sputtering of sample with Ar^+ ions liberate atoms, electrons and ions from the sample but atoms are excited and ionized by collisions with the plasma and detected by mass spectrometer or optical emission spectrometer (Figure 8 paper 37). rf-GDs is a powerful technique which can be used to analyze wide range of materials, conductive or not, bulk or multilayer [101]. It allows to analyze the elements including light ones like O, N and H, it has advantage over dc-GDs which is capability of use for both conducting and insulating materials.

References

1. P. Gyftou, E.A. Pavlatou, N. Spyrellis, *Appl. Surf. Sci*. 254 (2008) 5910.
2. Y.X. Gan, *Micron* 43 (2012) 782.
3. D.K. Singh, V.B. Singh, *Mater. Sci. Eng*. A 532 (2012) 493.
4. J.L. Stojak, J. Fransaer, J. B. Talbot, in: R.C. Alkire, D.M. Kolb (Eds.), Advances in Electrochemical Science and Engineering, Wiley-VCH Verlag, Weinheim, 2002.
5. R.K. Saha, T.I. Khan, *Surf. Coat. Technol*. 205 (2010) 890.
6. T. Lampke, B. Wielage, D. Dietrich, A. Leopold, *Appl. Surf. Sci*. 253 (2006) 2399.
7. F. Ebrahimi, G.R. Bourne, M.S. Kelly, T.E. Matthews, *Nanost. Mater*. 11 (1999) 343.
8. H. Ferkel, B. Müller, W. Reihemann, *Mater. Sci. Eng*. A 234 (1997) 474.
9. M.H. Fawsy, M.M. Ashour, A.M. Abd El-Halim, *Trans. Inst. Met. Finish*. 74 (1996) 72.
10. Z. Xiaowei, S. Yifu, Z. Yingying, J. Huiming, *J. Rare Earths* 29 (2011) 883.
11. W. Wang, F.Y. Hou, H. Wang, H.T. Guo, *Scripta Mater*. 53 (2005) 613.
12. I. Ul-Haq, T.I. Khan, *Surf. Coat. Technol*. 205 (2011) 2871.
13. K. Kumar, R. Chandramohan, D. Kalyanaraman, *Appl. Surf. Sci*. 277 (2004) 383.
14. M. Stroumbouli, P. Gyftou, E.A. Pavlatou, N. Spyrellis, *Surf. Coat. Technol*. 195 (2005) 325.
15. S.C. Wang, W.C.J. Wei, *Mater. Chem. Phys*. 78 (2003) 574.
16. P. Nowak, R.P. Socha, M. Kaisheva, J. Fransaer, J.P. Celis, Z. Stoinov, *J. Appl. Electrochem*. 30 (2000) 429.
17. G. Maurin, A. Lavanant, *J. Appl. Electrochem*. 25 (1995) 1113.
18. P. Gyftou, E.A. Pavlatou, N. Spyrellis, K.S. Hatzilyberis, *Trans. Inst. Met. Finish*. 78 (2000) 223.
19. P. Gyftou, M. Stroumbouli, E.A. Pavlatou, N. Spyrellis, *Trans. Inst. Met. Finish*. 80 (2002) 88.
20. M.A. Khazrayie, A.R.S. Aghdam, *Trans. Nonferrous Met. Soc. China* 20 (2010) 1017.
21. C.M.P. Kumar, T.V. Venkatesha, *Phys. Scr*. 86 (2012) 015804.
22. E. Pompei, L. Magagnin, N. Lecis, P.L. Cavallotti, *Electrochim. Acta* 54 (2009) 2571.
23. X.H. Chen, F.Q. Cheng, S.L. Li, L.P. Zhou, D.Y. Li, *Surf. Coat. Technol*. 155 (2002) 274.
24. N. Guglielmi, *J. Electrochem. Soc*. 119 (1972) 1009.
25. J.P. Celis, J.R. Roos, *J. Electrochem. Soc*. 134 (1987) 1402.
26. K. Kurozaki, *J. Jpn. Inst. Met*. (1979) 10.
27. J. Fransaer, J.P. Celis, J.R. Roos, *J. Electrochem. Soc*. 139 (1992) 413.
28. P.M. Vereecken, I. Shao, *P.C. Searson* 147 (2000) 2572.
29. P. Narasimann, M. Pushpavanam, V.M. Periasamy, *Appl. Surf. Sci*. 258 (2011) 590.
30. S.T. Aruna, V.K. William Grips, K.S. Rajam, *J. Appl. Electrochem*. 40 (2010) 2161.
31. C.T.J. Low, R.G.A. Willis, F.C. Walsh, *Surf. Coat. Technol*. 201 (2006) 371.

32. H. Natter, R. Hempelmann, *Electrochim. Acta* 49 (2003) 51.
33. H. Natter, R. Hempelmann, *J. Phys. Chem.* 222 (2008) 319.
34. M. Paunovic, M. Schlesinger, Fundamentals of Electrochemical Deposition, Wiley-Interscience Publication, John Wiley Sons, Inc., 1988, p. 197.
35. M.R. Vaezi, S.K. Sadrnezhaad, L. Nikzad, *Colloids Surf. A: Physico. Chem. Eng. Aspects* 315 (2008) 176.
36. G.N.K. Ramesh Bapu, S. Jayakrishnan, *Surf. Coat. Technol.* 206 (2012) 2330.
37. R. Sen, S. Das, K. Das, *Mater. Charact.* 62 (2011) 257.
38. A.M. Rashidi, A. Amadeh, *Surf. Coat. Technol.* 204 (2009) 353.
39. D.R. Turner, *J. Electrochem. Soc.* 100 (1953) 15.
40. A.M. El-Sherik, U. Erb, *J. Mater. Sci.* 30 (1995) 5743.
41. R.T.C. Choo, J. Toguri, A.M. El-Sherik, U. Erb, *J. Appl. Electrochem.* 25 (1995) 384.
42. J.P. Bonino, P. Pouderoux, C. Rossignol, A. Rousset, *Plat. Surf. Finish.* 79 (1992) 62.
43. T.C. Franklin, *Plat. Surf. Finish.* 84 (1994) 62.
44. D. Mockute, G. Bernotiene, *Surf. Coat. Technol.* 135 (2000) 42.
45. B. Szeptycka, *Russ. J. Electrochem.* 37 (2001) 684.
46. Y. Nakamura, N. Kaneko, M. watanabe, H. Nezu, *J. Appl. Electrochem.* 24 (1994) 227.
47. A. Bund, D. Thiemig, *Surf. Coat. Technol.* 201 (2007) 7092.
48. A. Bund, D. Thiemig, *J. Appl. Electrochem.* 37 (2007) 345.
49. C. Kollia, N. Spyrellis, *Surf. Coat. Technol.* 37 (1993) 7.
50. V.P. Gerco, W. Baldauf, *Plating* 55 (1968) 250.
51. R.W. Williams, P.W. Martin, *J. Trans. Inst. Met. Finish.* 42 (1964) 182.
52. M.R. Vaezi, S.K. Sadrnezhaad, L. Nikzad, *Colloids Surf. A: Physico. Chem. Eng. Aspects* 315 (2008) 176.
53. P. Baghery, M. Farzam, A.B. Mousavi, M. Hosseini, *Surf. Coat. Technol.* 204 (2010) 3804.
54. R. Sen, S. Das, K. Das, *Surf. Coat. Technol.* 205 (2011) 3847.
55. S.L. Kuo, Y. C. Chen, M.D. Ger, W.H. Hwu, *Mater. Chem. Phys.* 86 (2004) 5.
56. E. Pompei, L. Magagnin, N. Lecis, P.L. Cavallotti, *Electrochim. Acta* 54 (2009) 2571.
57. L.M. Wang, *J. Appl. Electrochem.* 38 (2008) 245.
58. E. Rudnik, L. Burzynska, L. Dolasinski, M. Misiak, *Appl. Surf. Sci.* 256 (2010) 7414.
59. R.F. Ehram, US patent 4, 043, 878.
60. K. Helle, Report AKZO Research, Arnhem (1993).
61. A. Hovestad, L.J.J. Jansen, *J. Appl. Electrochim.* 25 (1995) 519.
62. N.K. shrestha, I. Miwa, T. Saji, *J. Electrochem. Soc.* 148 (2001) C106.
63. M.D. Ger, *Mater. Chem. Phys.* 87 (2004) 67.
64. H. Gül, F. Kılıç, S. Aslan, A. Alp, H. Akbulut, *Wear* 267 (2009) 976.
65. N.K. Shrestha, M. Masuko, T. Saji, *Wear* 254 (2003) 555.
66. K. Izutsu, Electrochemistry in Nonaqueous Solutions, WileyVCH Verlag, Weinheim, 2002.
67. H. J. Gores, J.M.G. Barthel, *Pure Appl. Chem.* 67 (1995) 919.
68. T. Hirato, J. Fransaer, J. –P. Celis, *J. Electrochem. Soc.* 148 (2001) C280.
69. J. Fransaer, E. Leunis, T. Hirato, J.–P. Celis, *J. Appl. Electrochem.* 32 (2002) 123.
70. N.K. Shrestha, T. Saji, *surf. Coat. Technol.* 186 (2004) 444.
71. V.B. Singh, P. Pandey, *J. New Mater. Electrochem. Syst.* 8 (2005) 299.
72. A. Chiba, T. Ogawa, T. Yamashita, *Surf. Coat. Technol.* 34 (1988) 455.
73. A. Chiba, K. Kitamura, T. Ogawa, *Surf. Coat. Technol.* 27 (1986) 83.
74. N.D. Nikolic, H. Wang, H. Cheng, C.A. Guerrero, N. Garcia, *J. Magn. Magn. Mater.* 272 (2004) 2436.
75. X.P. Li, Z.J. Zhao, H.L. Seet, W.M. Heng, T.B. Oh, J.Y. Lee, *Electrochem. Solid State lett.* 7 (2004) C1.
76. Z. H. Gu, T.Z. Fahidy, *J. Phys. D: Appl. Phys.* 33 (2000) L113.

77. T. Yamada, S. Asai, *J. Jpn. Inst. Met*. 69 (2005) 257.
78. Q. Feng, T. Li, Z. Zhang, J. Zhang, M. Liu, J. Jin, *Surf. Coat. Technol*. 201 (2007) 6247.
79. Wang, Y. Zhong, W. Ren, Z. Lei, Z. Ren, J. Jia, A. Jiang, *Appl. Surf. Sci*. 254 (2008) 5649.
80. J.L. Stojak, J. Fransaer, J.B. Talbot, in: R.C. Alkire, D.M. Kolb (Eds.), *Adv. Electrochem. Sci*. Eng., Wiley-VCH Verlag, weinheim, 2002.
81. R.A. Tacken, L.J.J. Janssen, *J. Appl. Electrochem*. 25 (1995) 1.
82. P. Baghery, M. Farzam, A.B. Mousavi, M. Hosseini, *Surf. Coat. Technol*. 204 (2010) 3804.
83. K. M. Yin, *Surf. Coat. Technol*. 88 (1996) 162.
84. N. S. Qu, K. C. Chan, D. Zhu, *Surf. Coat. Technol*. 91 (1997) 220.
85. C. Yang, Z. Yang, M. An, J. Zhang, Z. Tu, C. Li, Plat. *Surf. Finish*. 88 (2001) 116.
86. P. Gyftou, M. Stroumbouli, E.A. Pavlatou, P. Asimidis, N. Spyrellis, *Electrochim. Acta* 50 (2005) 4544.
87. E.A. Pavlatou, M. Stroumbouli, P. Gyftou, N. Spyrellis, *J. Appl. Electrochem*. 36 (2006) 385.
88. C.T.J. Low, R.G.A. Wills, F.C. Walsh, *Surf. Coat. Technol*. 201 (2006) 371.
89. I. Garcia, J. Fransaer, J. P. Celis, *Surf. Coat. Technol*. 148 (2001) 171.
90. A.F. Zimmerman, D. G. Clark, K.T. Aust, U. Erb, *Mater. Lett*. 52 (2002) 85.
91. G. Heidari, H. Tavakoli, S.M.Mousavi Khoie, *J. Mater. Eng. Perform*. 19 (2010) 1183.
92. Guo, X. Y. Zhu, R.D. Xu, *Acta Metall. Sin*. 20 (2007) 111.
93. R. Sen, S. Das, K. Das, *Mater. Res. Bull*. 47 (2012) 478.
94. A. Jung, H. Natter, R. Hempelmann, E. Lach, *J. Mater. Sci*. 44 (2009) 2725.
95. M.E. Bahrololoom, R. Sani, *Surf. Coat. Technol*. 192 (2005) 154.
96. L. Chen, L. Wang, Z. Zeng, T. Xu, *Surf. Coat. Technol*. 201 (2006) 599.
97. R. Sen, S. Das, K. Das, *Metall. Mater. Trans*. A 42 (2011) 1409.
98. R. Sen, S. Bhattacharya, S. Das, K. Das, *J. Alloys Compd*. 489 (2010) 650.
99. X. Xe, J.P. Celis, M. De Bonte, J. R. Roos, *J. Electrochem. Soc*. 141 (1994) 2689.
100. M. Lekka, C. Zanella, A. Klorikowska, P.L. Bonora, *Electrochim. Acta* 55 (2010) 7876.
101. A. Lanzutti, E. Marin, M. Lekka, P. Chapon, L. Fedrizzi, *Surf. Interface Anal*. 44 (2012) 48.